3D Modelling of Electromagnetic Time Reversal

Localization of a dielectric object in a half-space

Mehdi Benhamouche
Laboratoire de Génie Electrique de Paris, UMR 8507 CNRS, SUPELEC, Université Paris-Sud, UPMC
11 rue Joliot-Curie
91192 Gif-sur-Yvette cedex, France
mehdi.benhamouche@supelec.fr

Laurent Bernard
Laboratoire de Génie Electrique de Paris, UMR 8507 CNRS, SUPELEC, Université Paris-Sud, UPMC
11 rue Joliot-Curie
91192 Gif-sur-Yvette cedex, France
laurent.bernard@lgep.supelec.fr

Lionel Pichon
Laboratoire de Génie Electrique de Paris, UMR 8507 CNRS, SUPELEC, Université Paris-Sud, UPMC
11 rue Joliot-Curie
91192 Gif-sur-Yvette cedex, France
lionel.pichon@lgep.supelec.fr

Dominique Lesselier
Laboratoire des Signaux et Systèmes, UMR 8506 CNRS, SUPELEC, Université Paris-Sud
3 rue Joliot-Curie
91192 Gif-sur-Yvette cedex, France
dominique.lesselier@lss.supelec.fr

ABSTRACT

This paper presents a 3D full time-domain modelling of the time reversal process for the localization of a dielectric obstacle buried in an homogeneous half-space using an array of dipoles. The main purpose of this study is to propose a localization method based on the analysis of the ElectroMagnetic (EM) energy of the back-propagated fields. A Generalized Finite Difference (GFD) method and a leapfrog time discretization are used to get the numerical results.

Categories and Subject Descriptors

D.2.8 [**Software Engineering**]: Metrics—*complexity measures, performance measures*.

General Terms

Algorithms

Keywords

3D full time-domain Maxwell's equations, time reversal (TR), localization of dielectric scatterers.

1. INTRODUCTION

Time Reversal (TR) techniques have firstly been used in an acoustic context [1] and more recently have been applied to several electromagnetic applications such as wireless communication [2], generation of high-field intensity pulses [3], and localization of scatterers [4]. In a lossless medium Maxwell's equations are time-symmetric, so a time-reversed electromagnetic field is expected to go back toward the sources. Since an obstacle illuminated by a given EM wave can be considered as a set of secondary sources within it (or at its surface), it is then expected that the TR of the scattered field converges toward the obstacle (in some sense, to be considered further).

Localization or imaging of dielectric obstacles by decomposition of the time reversal operator (DORT) [5] has been recently studied theoretically [6] and experimentally [7] using separate transmit and receive arrays. The DORT method is based on the harmonic measurement of the response matrix and the analysis of its singular value decomposition. Here, we are interested in full time domain analysis of the time reversed fields.

One of the difficulties of the time-domain approach is to determine the time focusing time. For 2D problems, one may be able to find this focusing time by observing the distribution of the fields during the time reversed simulation [8] [9]. A method based on a minimum entropy criterion for the electric field was proposed in a 2D electric transverse example to localize breast cancer [4]. According to the authors, this method is quite robust with respect to the signal input. For 3D problems, an objective method must be used to find this focusing time. Here we propose an alternative one essentially based on the time and space analysis of the

NCMIP 2011, May 25, Paris, France

DOI 10.4108/icst.valuetools.2011.245818

density of electromagnetic energy in an appropriate interval of time and a given research space domain.

2. TIME DOMAIN SIMULATION METHOD

The Generalized Finite Difference (GFD) method [10] provides a general framework for the mesh-based numerical methods such as finite elements (FE) or finite integration technique (FIT) [11], enabling us to handle unstructured meshes. Using unstructured meshes with GFD leads to better dispersion properties compared to classical Finite Difference Time Domain (FDTD) as employed in most 3D time-domain simulations. A leapfrog scheme is used for the time-domain discretization, and truncation of the computational domain via perfectly matched layers yields simulation of the infinite free space (and/or half-space) [13].

In practice, the box containing the obstacle and the surrounding free space is spatially discretized on an unstructured tetrahedral mesh (the same mesh will be used for all configurations considered in the analysis here). One face of the box is meshed with structured triangles in order to model the array of dipoles: any edge of this mesh could be chosen as an active dipole of the array, and density and polarization managed by an appropriate choice of a set of active edges. When simulating the direct problem, some edges of the array are used to generate the EM pulse. The other ones are then used to collect the received signals. The signal, corresponding to the scattered field contribution of the object, is computed by difference of the received signals in two configurations: half-space only, and obstacle embedded in half-space. The TR field in half-space follows by the back-propagation of the TR received signals from all active edges, using the same time scheme as in the direct simulation.

This approach is used as such since the EM features of the ground are *a priori* well known and can thus be modeled as in [4]. The main wave front of TR field is expected to focus only onto the sought source (object), the half-space being expected of minor effect since the signal contribution of the scatterer in the system has been isolated.

3. PROBLEM CONFIGURATION

A non-conducting dielectric ellipsoid with relative permittivity ϵ_r^{object} centred at (0.075 m, 0.2 m, 0.5 m) with semi-axis lengths $r_x = 0.3$ m, $r_y = r_z = 0.2$ m is illuminated by a y-polarized electric dipole placed at the center of the array of dipoles.

A gaussian ElectroMotive Force (EMF) defined by,

$$V(t) = V_0 \ \exp(-(c_0(t - t_0))^2), \qquad (1)$$

with $c_0 = 3\ .10^8\,\mathrm{m\,s^{-1}}$ and $t_0 = \frac{6}{c_0}$ s, is applied along the dipole. The ellipsoid is buried into a half-space, defined by $x \leqslant 1.5$ m, of relative permittivity $\epsilon_r^{half-space}$. The transmitter dipole has the same length (0.125 m) and the same polarization than the transceiver dipoles, used as a TR array. This array is composed by 7×7 dipoles uniformly distributed over the rectangular surface defined by (2.25 m, −1.625 m, −1.5 m) and (2.25 m, 1.625 m, 1.5 m). See Figure 1.

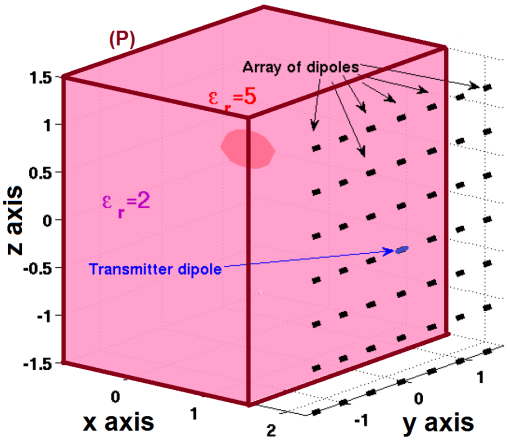

Figure 1: 3D view of the configuration

4. COMPUTATIONAL PROCEDURE

Firstly, the direct problem (I) is solved by transmitting the signal pulse (by the transmitter dipole) in the presence of the half-space ($\epsilon_r^{object} = 2$, $\epsilon_r^{half-space} = 2$, Figure 2). The induced EMFs $V_{d\in D}^{t1}(t)$, corresponding to the total electric field, are recorded by each transceiver dipole d during an interval of time $[0\ M_t]$ ($c_0 M_t = 30$ m). Then, another direct problem (II) is solved by transmitting the same signal pulse with the same transmitter dipole in the presence of the half-space including the buried scatterer ($\epsilon_r^{object} = 5$, $\epsilon_r^{half-space} = 2$, Figure 2).

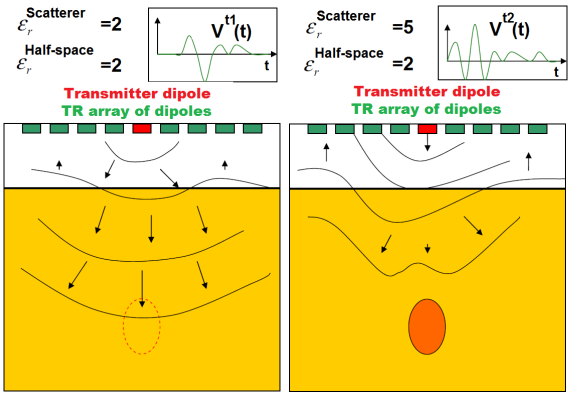

Figure 2: Scheme of direct problems I (left) and II (right)

The induced EMFs $V_{d\in D}^{t2}(t)$, corresponding to the total electric field are recorded by the transceiver dipoles during the same time interval $[0\ M_t]$. In an experimental configuration, these signals would be given by two measurements; then, $V_{d\in D}^{\Delta}(t) = V_{d\in D}^{t2}(t) - V_{d\in D}^{t1}(t)$ are computed. This difference corresponds to the scattered field contribution. These signals ($V_{d\in D}^{\Delta}(t)$) are time reversed and applied as EMF on the dipole array to illuminate the half-space. This procedure is justified by writing and analysing Maxwell's equations for the scattered field contribution, as exposed below.

4.1 Maxwell's equations for the total fields

Let (ϵ_1, μ_1) and (ϵ_2, μ_2) be the spatial distributions of the electric permittivity and the magnetic permeability on, re-

spectively, the direct problem (I) and(II). Maxwell's equations for the total field are:

$$\text{curl}\,(e_i) = -\frac{\partial b_i}{\partial t},\ \text{curl}\,(h_i) = \frac{\partial d_i}{\partial t}, \tag{2}$$

$$d_i = \epsilon_i e_i,\ b_i = \mu_i h_i, \tag{3}$$

$$u_d.e_i\ |_d = V(t). \tag{4}$$

$i = 1, 2$, for, respectively, the direct problem (I) and (II). u_d is the unit vector chosen according to the orientation of the transmitter dipole. e_i, h_i are respectively the total electric and magnetic fields, d_i, b_i are, respectively the displacement current and the magnetic flux density.

4.2 Maxwell's equations for the scattered fields

Define $e_\Delta = e_2 - e_1$, and by the same way h_Δ. Define also $d_\Delta = \epsilon_i e_\Delta$, $b_\Delta = \mu_i h_\Delta$. The equivalent system is:

$$\text{curl}\,(e_\Delta) = -\frac{\partial b_\Delta}{\partial t} + J_M,\ \text{curl}\,(h_\Delta) = \frac{\partial d_\Delta}{\partial t} + J_E, \tag{5}$$

$$d_\Delta = \epsilon_i e_\Delta,\ b_\Delta = \mu_i h_\Delta \tag{6}$$

$$u_d.e_\Delta\ |_d = 0, \tag{7}$$

with $J_M = -\mu_\Delta \frac{\partial h_j}{\partial t}$, $J_E = \epsilon_\Delta \frac{\partial e_j}{\partial t}$, $\epsilon_\Delta = \epsilon_2 - \epsilon_1$, $\mu_\Delta = \mu_2 - \mu_1$, $(i, j) = (1, 2)$ or $(2, 1)$. It can be noted that J_M and J_E are null except in the volume of the object. So, the problem is equivalent to solve Maxwell's equations for the scattered field with permittivity and permeability distributions $(\epsilon_i,\ \mu_i)$ and current sources.

The choice of $(i, j) = (1, 2)$ or $(2, 1)$ has no effect since $\epsilon_1 = \epsilon_2$ and $\mu_1 = \mu_2$ outside the object and only the formulation of the current sources differs. In both cases, the volume of the object represents an equivalent EM source of field which is observed by the array of dipoles. This formulation of Maxwell's equations and the TR principle allow to justify the back-propagation of the TR signals $V^{\Delta}_{d\in D}(M_t - t)$ towards the half-space in order to focus onto the sought source (ellipsoid).

5. LOCALIZATION METHOD

For each time step, the EM energy is calculated within a region P of the half-space (rectangular parallelepipedic half-space part of the computational domain where the scatterer is searched, here defined by $(-0.875\,\text{m}, -1.625\,\text{m}, -1.5\,\text{m})$ and $(1.5\,\text{m}, 1.625\,\text{m}, 1.5\,\text{m})$). The EM energy in P is obtained from the constitutive matrices, the discrete induction fluxes and electromotive forces [11]. The density of energy $\rho = \frac{1}{2}(\varepsilon e^2 + \mu h^2)$ is computed at $27 \times 27 \times 27$ nodes $n_{j\in J}$ of an uniform grid G covering P. Then, only the set T of time steps $t_{i\in I}$ for which the EM energy in P is greater than 50 % of its maximum is considered. For each time step $t_i \in T$, the set of nodes $n_{j\in J}$ of G is classified into K subsets $(S^i_1, S^i_2, ..., S^i_K)$, according to their densities of EM energy (ρ^i_j), see Figure 3. For any k, $1 \le k \le K$:

$$\forall j \in J \quad n^i_j \in S^i_k \Leftrightarrow \rho^i_j \in \left]\frac{k-1}{K}\rho^i_{max}, \frac{k}{K}\rho^i_{max}\right]. \tag{8}$$

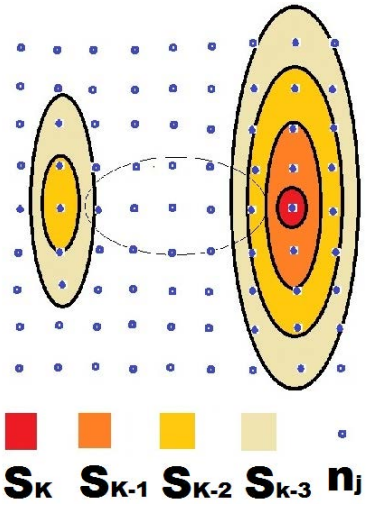

Figure 3: A 2D view of density regions of EM energy

So, a contrast of $\frac{100}{K}$ % of the maximum density of EM energy (ρ^i_{max}) (recorded every time step) is chosen to separate the density regions of EM energy. Let N^i_k be the number of nodes at the time step t_i in the set S^i_k. We define the set T_K of time steps t_{i_K}such that $t_{i_K} = \arg\min_{t_i\in T}(N^i_K)$. If there is a unique solution t_{i_K}, the focusing time is $t_f = t_{i_K}$. Otherwise, for $p \ge 1$, we recursively define T_{K-p} the set of time steps $t_{i_{K-p}}$such that

$$t_{i_{K-p}} = \underset{t_i\in T_{K-p+1}}{\arg\min}\ (N^i_{K-p}), \tag{9}$$

until the solution $t_{i_{K-p}}$ is unique or $p = K - 2$, then $t_f = t_{i_{K-p}}$, $t_{i_{K-p}} \in T_{K-p}$.

The above procedure can be summarized as follows: once defined the search domain, one subdivides at each time step the density distribution of EM energy into a given number of volume regions K using a linear contrast. Then, one considers that the time of focus at the equivalent sources is the time when the region of maximum density of EM energy is localized within the smallest volume. It is selected among such time steps for which the EM energy in P is sufficiently high, in order to eliminate those when the back-propagated wave fronts start to penetrate into the search space. That is, time steps for which the density distribution of EM energy is located (in a small volume) at the boundary of the search domain are not taken into consideration.

6. NUMERICAL RESULTS

During the TR simulation, the EM density of energy is computed at each point of the grid G every 13 time steps, which corresponds to an interval of time Δt_{EM} , $c_0 \Delta t_{EM} = 0.03\,\text{m}$. The EM energy in P is also computed at the same time steps as the EM density of energy. After that, the localization method is applied using the information about time variation of the EM energy in P and EM density in G, to determine the times of focus. In the given example, $K = 6$ is chosen, but almost the same results are obtained for the values of K between 4 and 50. The time variation of the number of points N_k, $k = 3, 4, 5, 6$, is sketched in Figure 4. In general, the method can yield several times of focalization and in case of neighbouring time steps, their mean value is chosen.

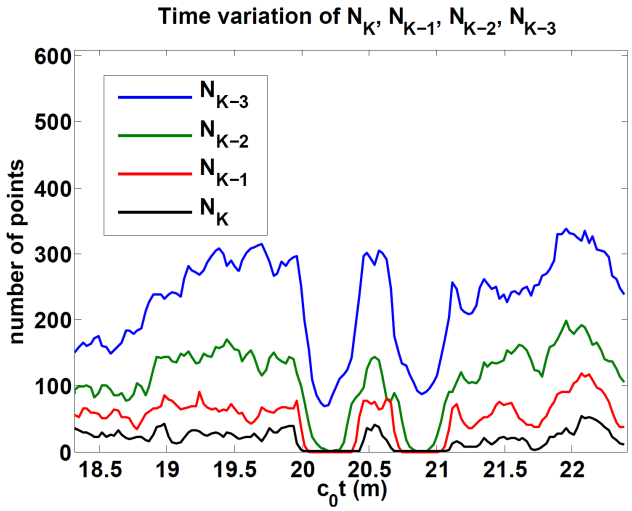

Figure 4: Time variation of number of points when using $K = 6$

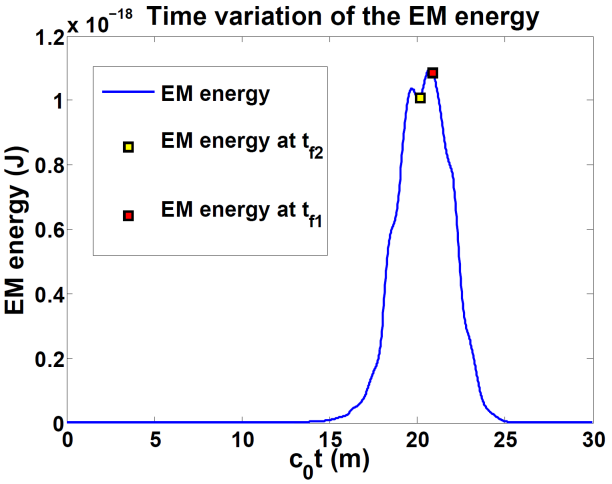

Figure 5: Time variation of the EM energy in P

The time of focalization given by the algorithm is unique as for all the other cases from $K = 5$ to $K = 50$. The unique time obtained is $t_{f_1} = \frac{1}{c_0} 20.89\,\text{s}$, except in two cases ($K = 5, 7$) for which the unique result is $t_{f_2} = \frac{1}{c_0} 20.22\,\text{s}$. For any value of $K = 5, 6, .., 50$, the distributions of the points n_j in S_k regions, at these time steps (t_{f_1}, t_{f_2}), are almost similar. The algorithm hardly selects one of them, as the time of focalization, after more than 3 iterations ($p \geqslant 3$).

On the interval of time $]t_{f_2}, t_{f_1}[$ the volumes of the regions S_k, $k = 6, 5, 4, 3$, increase simultaneously; afterwards they decrease to reach their minimum at t_{f_1} (Figure 4). These times, are not far from the one when the EM energy in P reaches its maximum (Figure 5). The normalized EM density of energy at $n_j \in G$, defined by

$$\nu_j^i = \frac{\rho_j^i}{\max_{\substack{i \in I \\ j \in J}} \rho_j^i}, \tag{10}$$

is computed at these times of focus in order to illustrate the distribution of the EM density of energy, refer to Figures 6 and 7.

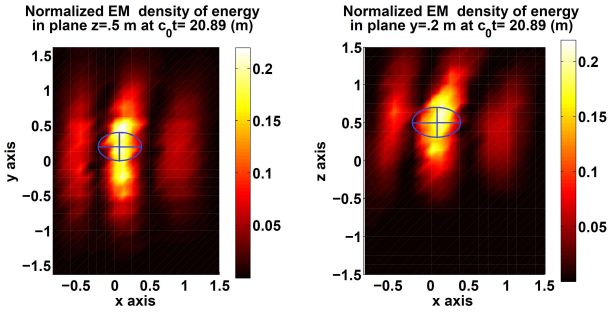

Figure 6: Density of EM energy at t_{f_1}

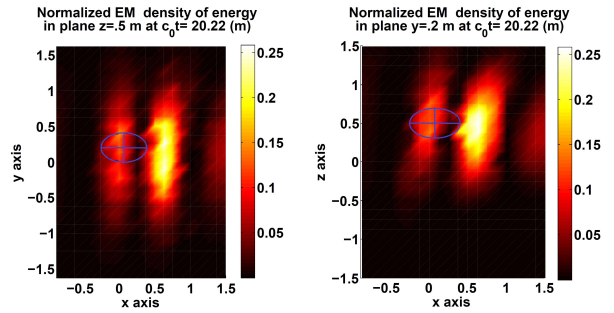

Figure 7: Density of EM energy at t_{f_2}

It can be noticed that the normalized EM density of energy observed in P at t_{f_2} is larger than the one observed at t_{f_1}. At t_{f_2}, the main wave front focusing approximatively near the side of the ellipsoid exposed directly to the transmitter dipole; but at t_{f_1}, it focuses rather into the interior of the ellipsoid.

7. CONCLUSION AND PERSPECTIVES

The proposed method has proved its robustness according to its main parameter K (number of density regions of EM energy chosen) for the localization of a buried object in an homogeneous media. This method uses information about EM density but it could also use time and space distributions

of the TR electric or magnetic fields; it also allows to localize the scatterer.

It is expected that the method should provide similar results for a magnetic ellipsoid. The localization of a metallic (perfectly conducting) one certainly deserves more investigation, even though localization might be improved in view of secondary sources found at its surface only and possibly subsequent focalization onto this surface. Further works will address the application of the method for the localization of more extended objects and the test of the robustness of the method in random heterogeneous media.

8. REFERENCES

[1] M. Fink, D. Cassereau, A. Derode, C. Prada, P. Roux, M. Tanter, J. Thomas, and F. Wu, "Time-reversed acoustics," Reports on Progress in Physics, Vol. 63, p. 1933-1995, 2000.

[2] Xiao, J. Chen, B.-Z. Wang, and X. F. Liu, "A numerical study on TR electromagnetic wave for indoor ultra-wideband signal transmission," PIER, Vol. 77, p. 329-342, 2007.

[3] M. Davy, J. de Rosny, J.-C. Joly, M. Fink, "Focusing and amplification of electromagnetic waves by time reversal in an leaky reverberation chamber," Comptes Rendus Physique, Vol. 11, p. 37-43, 2010.

[4] P. Kosmas and C. M. Rappaport, "Time reversal with the FDTD method for microwave breast cancer detection," IEEE Transactions on Microwave Theory and Techniques, Vol. 53, p. 2317-2323, 2005.

[5] E. Iakovleva and D. Lesselier , "Multistatic response matrix of spherical scatterers and the back-propagation of singular fields," IEEE Transactions on Antennas and Propagation, Vol. 56, p. 825-833, 2008.

[6] J.-G. Minonzio, M. Davy, J. de Rosny, C. Prada, and M. Fink, "Theory of the time-reversal operator for a dielectric cylinder using separate transmit and receive arrays," IEEE Transactions on Antennas and Propagation, Vol. 57, p. 2331-2340, 2009

[7] M. Davy, J.-G. Minonzio, J. de Rosny, C. Prada, and M. Fink, "Experimental study of the invariants of the time-reversal operator for a dielectric cylinder using separate transmit and receive arrays," IEEE Transactions on Antennas and Propagation, Vol. 58, p. 1349-1356, 2010

[8] N. Maaref, P. Millot, X. Ferrières, C. Pichot, and O. Picon, "Electromagnetic imaging method based on time reversal processing applied to through-the-wall target localization," PIER, Vol. 1, p. 59-67, 2008.

[9] M. E. Yavuz, and F. L. Teixeira, "A numerical study of time-reversed UWB electromagnetic waves in continuous random media," IEEE Antennas and Wireless Propagation Letters, Vol. 4, p. 43-46, 2005.

[10] A. Bossavit, "Generalized finite differences in computational electromagnetics," PIER, Vol. 32, p. 45-64, 2001.

[11] M. Clemens and T. Weiland, "Discrete electromagnetism with finite integration technique," PIER, Vol 32, p. 65-87, 2001.

[12] M. E. Yavuz, and F. L. Teixeira, "Full time-domain DORT for ultrawideband electromagnetic fields in dispersive, random inhomogeneous media," IEEE Transactions on Antennas and Propagation, Vol. 54, p. 2305-2315, 2006.

[13] L. Bernard, R. Torrado, L. Pichon, "Efficient implementation of the UPML in the generalized finite-difference time-domain method," IEEE Transactions on Magnetics, Vol. 46, p. 3492-3495, 2010.